ACCELERATED LIFE CONSUMPTION DUE TO THERMO-ACOUSTIC OSCILLATIONS IN GAS TURBINES: XFEM & CRACK

A. Can Altunlu*†, Peter van der Hoogt*, André de Boer*

*** Faculty of Engineering Technology, University of Twente, P.O. Box 217, 7500 AE Enschede, the Netherlands**

email†: *a.c.altunlu@utwente.nl*

Keywords: *gas turbine, combustion dynamics, life assessment, crack, xfem*

Abstract

The combustion instability phenomenon in the gas turbine engines brings out elevated vibrations under high temperature levels. The present work addresses the projection of a life assessment methodology applied in a laboratory-scaled generic combustor onto the typical gas turbine engine combustor section in terms of crack and its evaluation. A temperature-structural analysis based on the combustion experiments was utilized to obtain the crack initiation region. Sequentially coupled extended finite element method (XFEM) based fracture mechanics analysis was performed to characterize the crack-tip near fields in a typical combustor nickel-based superalloy.

1 Introduction

Land-based gas turbine engines are devoted to the advancements in terms of efficiency and emissions. The engines are intended to be working at the designed performance levels during their service life. During their lifetime the engines can experience various operation scenarios due to the need of flexible energy output. Particularly, the combustor section components experience severe loading conditions and history to meet these output requirements. Complex damage phenomena such as high cycle fatigue, low cycle fatigue, creep can be induced and interact during the service. Hence, reliable analysis on not only the initiation of cracks/flaws but also the growth process can play a significant role in the total life assessment of gas turbine critical components that operates under complex loading histories and lead to achieve safety and integrity targets[1-3]. The remaining lifetime of the damaged critical components is strongly depended on the loading history such as the stress levels, temperature profiles or loading frequency that can lead to an accelerated crack growth rate or retardation.

In this paper, the dynamic two-way interaction between the oscillating pressure load in the fluid and the motion of the structure under limit-cycle conditions due to the thermo-acoustic instabilities in a generic combustor was experimentally investigated. Following, the experimental measurements on the combustion instabilities were extended towards numerical integrated remaining life assessment by fracture mechanics analysis. The and the stress-field ahead of the crack tip was characterized including fatigue and creep aspects.

The following sections describes the methodology and the procedure and the theory of the multidisciplinary approach. In the subsections the combustor test system and the test materials are detailed and thermal-structural coupled analysis is described. Next the fatigue crack growth (FCG) and the creep crack growth (CCG) theory and the proposed method for residual lifing using XFEM is described. In section 3 the results are presented and the conclusions and discussions are included in the last section.

2 Methodology & multidisciplinary analysis

Multidisciplinary domains were inter-linked throughout this work including combustion, acoustics, structural dynamics, fracture mechanics and life assessment. The schemata of the investigation presented in this paper is depicted in Figure 1. The physical based two-way interaction during the unstable combustion inside the test combustor was utilized experimentally in a generic laboratory-scaled combustor. The loading history generated by the combustion process was measured including the cyclic pressure, temperature profile and the combustion characteristic frequency. The measurements were post-processed and imported as the loading condition in the thermal-structure coupled finite element analysis to predict the stress concentration zones. The fracture mechanics analysis was performed to calculate the crack driving parameters assuming that the crack initiated from the pre-existing defects located in the stress concentration zones. Identical to the service conditions in the industrial gas turbine engines, the crack growth was governed by the fatigue and creep mechanisms in the numerical analysis.

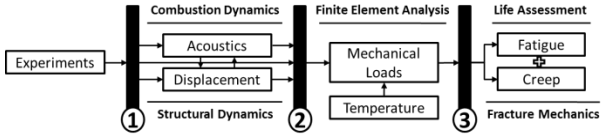

Figure 1. The schemata of the investigation

2.1 Combustor test system

The laboratory-scaled generic combustor test system is depicted in Figure 2. The measurement locations are designated as "p#" that are the pressure, fluid temperature and the liner wall vibration. The Rijke tube type combustor mainly consists of two sections; the upstream (S1) and downstream (S2&S3). In Figure 3, the full geometry (a), the flame-box configuration (b) and the wedge location and geometry (c) are visualized. The upstream section includes an air-feeding box, a rectangular duct and an equilateral triangular wedge that is detailed in the figure (c). The wedge acting as the flame holder intakes the fuel (methane) from the side holes (black-arrows) and sprays out the fuel from the small holes (red-arrows). Thus, the fuel and the air flowing upwards along the duct (blue-arrow) constitute a homogeneous mixture and the initiation takes place to form the flame. The downstream consists of a rectangular liner (S3) and a flame box (S2). The flame box detailed in Figure 3 (b) is enclosed by four quartz glasses (3), sandwiched by two gaskets (1) and mounted to the flame box by the frames (2). The quartz glasses (4 mm thick) can be replaced with the identical sized rectangular metal plates (1 mm thick) that can behave as one part together with its parent combustor structure. Hereafter the metal plate will be called as the specimen. During the experiments, the specimen replaced with one front quartz glass and the side windows are used to visualize the flame shape. Note that the flame stabilization takes place on the wedge wake and the generated turbulent flame is technically premixed.

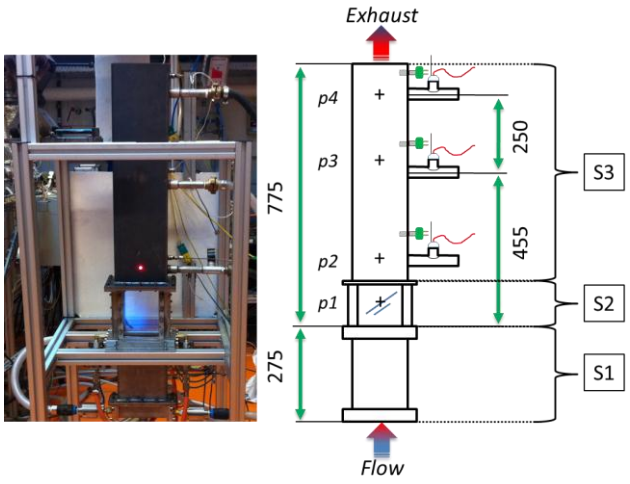

Figure 2. Combustor test system configuration

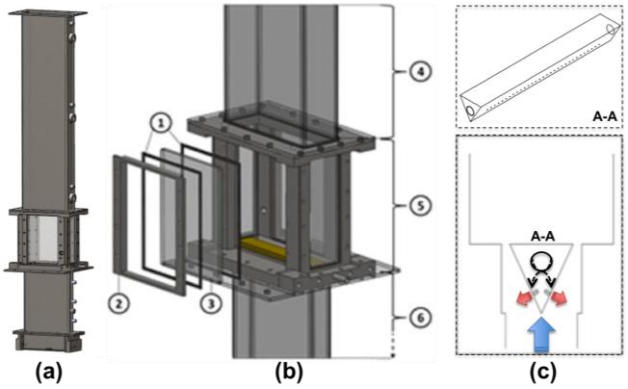

Figure 3. Flame-box configuration

2.2 Materials and compliance

The combustor test system is composed of austenitic stainless steel AISI-type 310 and 316 (specimen). The materials were selected due to the well-published properties and the sufficiently enough heat and corrosion resistance relative to the test temperatures and durations. The test combustor materials have analogous thermal and mechanical properties to the typical gas turbine combustion liner material, Haynes 230 nickel-based superalloy. Haynes 230 is superior due to its high temperature strength, high resistance to oxidizing environments (up to 1150 ^{o}C), long-term thermal stability and low thermal expansion characteristics [4]. The experimental output is numerically applied to Haynes 230 material to direct a projection towards a realistic lifing within an industrial perspective.

2.3 Finite element model

In the combustor finite element model as seen in Figure 7, five sections were included, (1) the downstream, (2) the upstream, (3) the specimen and quartz glasses, (4) the gaskets and (5) the welding. The material properties for each section are correspondingly, (1) AISI310, (2) AISI316, (3) AISI316 and fused quartz, (4) muscovite mica and (5) SS310 with higher young's modulus to satisfy the welding stiffness. The finite element mesh was generated using quadratic elements (tetrahedron, hexahedron, wedge and pyramid). Two elements were created across the liner wall and the specimen thickness and a finer mesh is used for the welding parts to accommodate the mesh compliance. A temperature-structural analysis was performed to calculate the stress and strain distributions. The applied loads and the boundary conditions are detailed flowingly.

Two FEM analysis were performed for the full geometry and for the specimen geometry only. In this manner, a benchmark numerical test was performed to reduce the computation cost. Hereby the full geometry analysis and the specimen geometry only analysis will be called as the full-model and sub-model analysis, respectively. In the full-model, a fully fixed support boundary condition (clamped) at the bottom of the flame box was applied. This support locations represents the scaffolding-like frame that holds the test system as seen in Figure 2 (left). And the experimentally measured pressures and surface temperatures were defined as the external data with respect to the dimensions of the geometry. Prior to the computation, the data were mapped and matched on the finite element mesh (point cloud data mapping).

In the experiments, the combustion process generates a varying surface temperature and thermal expansion condition at the downstream part that can induce pre-stress effects. Therefore, the assembly of the specimen to the flame-box is designed such that a clearance is present in the housing. This provides some freedom for the attached specimens to slide towards traverse and longitudinal directions. Furthermore, two gaskets (2 mm thick) accommodated on both sides of the specimen to compensate the third dimension of the volumetric expansion. Hence, the stresses in the specimen are assumed to be mainly covered by the pressure inside the combustor. In the numerical sub-model, the boundary conditions were modelled with an elastic foundation. This elastic support represents the gaskets that sandwich the specimen. Basically, a spring stiffness per unit area was represented by so-called the elastic foundation stiffness (EFS) [5]. EFS was applied on the in-plane and the out-of-plane faces of the support area. This provides a resistance to the direction normal to the volumetric expansion of the geometry. In this way, the sub-model can expand due to the thermal load and can deform out-of-plane direction due to the pressure load. The effects of the temperature and damping were assumed to be negligible for the EFS that is analogical with the gaskets material. Since the loads don't vary at the flame-box region as seen Figure 7 (a) and (b), a constant temperature and pressure were applied to the model.

2.4 Fracture mechanics model

The lifetime of combustion liners are potentially consumed by fatigue and creep mechanisms,

however their interaction also must be resolved for the crack growth assessment. In the next subsections the crack growth characterizing parameters for fatigue and creep are described. Furthermore, their interaction is formulated to govern the lifing and the usage of the proposed method in the XFEM framework is described.

2.4.1 Cycle-dependent fatigue crack growth

Typically the crack growth is associated with the strain energy release that is analogous to the dissipated energy to create new fracture surfaces. The components subjected to a cyclic load in the creep-temperature regime can undergo in the stages of the continuous evolving deformation zone ahead of the crack tip according to its stress-strain-time response [6]. If the plastic zone is small compare with the crack size, in other words the material experiences small-scale yielding at the crack tip, the energy release is in fact the *J*-integral [7, 8]. The *J*-integral is defined in the general form as:

$$J = \int_{\Gamma} \left(W dy - \boldsymbol{T}.\frac{\partial \boldsymbol{u}}{\partial x} ds \right) \quad (1)$$

$$W = \int_0^{\varepsilon_{ij}^m} \sigma_{ij} : d\varepsilon_{ij}^m \quad (2)$$

where Γ is a curve enclosing the crack tip in a counter-clockwise direction, W is the mechanical strain energy density varying with the stress, σ_{ij} and the mechanical strain, ε_{ij}^m, $\boldsymbol{T}$ is the traction vector on Γ defined according to the outward normal as $T_i=\sigma_{ij}n_j$, n_j is the vector of the outward unit normal n to the curve Γ, $\boldsymbol{u}$ is the displacement vector, and ds is an element of Γ. The *J*-integral, or strain energy release rate, is related to the stress intensity factor (SIF) for the linear-elastic materials as:

$$J = \eta \frac{1}{E}(K_I^2 + K_{II}^2) + \frac{1}{2G} K_{III}^2 \quad (3)$$

where $\eta=(1)$ for plane stress and $\eta=(1-\nu^2)$ for plane strain, E and ν are the Young's Modulus and the Poisson's ratio and $K_{I,II,III}$ are the fracture modes.

2.4.2 Time-dependent creep crack growth

Materials used in gas turbine engine combustors at elevated temperatures show superior creep strength and creep ductility. However, in the presence of a growing crack these materials can fail with exhibiting even very small bulk creep deformation. In general, the materials experienced CCG can be categorized as creep-ductile or creep-brittle. Previous studies showed that the austenitic steels behave creep-ductile at relatively lower temperatures (538^{o}C) [9, 10], whereas the nickel-based superalloys show creep-brittle behaviour at higher temperatures (927^{o}C) [11-13].

In creeping materials, three stages are defined for crack propagation by means of the size of the crack tip creep zone relative to the specimen dimensions that are small scale, transient and steady-state [14-16]. The state of stress at the crack tip can be characterized by a crack-tip parameter, which drives the approach from idealized laboratory specimens to the actual components acting as a transfer function [17, 18]. However there is no one unique parameter that can be used in all circumstances [19]. Therefore, the asymptotic solutions for the stresses in the creep zone, obeying the power-law creep of deformation, needs to be analysed implying that whether the SIF value is valid in the creep zone calculation [20]. Lu et al. [12] showed that a typical combustor material, Haynes 230, behaves as a creep-brittle material, of which the accumulated creep strains and the near-tip elastic strains around the crack are at comparable levels. Hence, assuming small scale yielding C_t-integral is can be utilized as a crack tip parameter and the time-dependency of the fracture mechanics can be included [21-23]. The C_t-integral can be defined by replacing the strains with strain rates and the displacements with the velocities, thus the mechanical strain energy density with the mechanical strain energy rate density, in the *J*-integral description. In the general form the strain energy rate density is described as:

$$\dot{W} = \int_0^{\dot{\varepsilon}_{ij}^m} \sigma_{ij} : d\dot{\varepsilon}_{ij}^m \quad (4)$$

Under secondary power law creep, the C_t-integral parameter can be described in terms of the stress intensity factor (K_C) for small-scale creep condition as:

$$C_t = \frac{1}{(n+1)t} \eta \frac{K_C^2}{E} \quad (5)$$

where n is the power law constant, t is the time. The reader is referred to the references for

detailed information on the formula derivation [20, 24-27].

2.4.3 Life assessment

The interaction of the cycle-dependent fatigue crack growth and the time-dependent creep crack growth were utilized using a linear summation model [28]. The model in general form is described as [29]:

$$\left(\frac{da}{dN}\right)^t = \left(\frac{da}{dN}\right)^f + \int \left(\frac{da}{dt}\right)^c \mathrm{dt} \quad (6)$$

where *a* is the crack length, *N* is the number of load cycles, *t* is the time, and the superscripts *t, f, c* are total, fatigue and creep, respectively. Lu et al. [12] showed that the fatigue-creep crack growth can be described by Paris-Erdogan law type formulation including only the C_t parameter. The formulation represents he crack growth behaviour of two solid solution strengthened superalloys, Haynes® 230 and Hastelloy® X alloys including hold-time effects and temperatures in the range of 816 and 927 ^oC. The crack growth rate is defined as follows:

$$\left(\frac{da}{dt}\right) = 0.0447(C_t)^{0.864} \quad (7)$$

The Eq. (7) is based on the tests following a baseline triangular waveform of 0.33 Hz. However, when a complex loading conditions are present such as varying loading ratios and frequencies, the behaviour of the crack growth can exhibit dependencies on these parameters [30]. In Eq. (6), the total crack growth rate is composed of the FCG rate relevant to a hold-time test and CCG rate during one cycle that is $\Delta t = 1/w + t_{hold}$, where *w* is the frequency of the waveform and t_{hold} is any hold time (dwell period). In the previous sections, the FGC and the CCG were expressed relevant to the SIF and thus *J*-integral. The total crack growth rate can be expressed as Paris-Erdogan law type formulation as:

$$\left(\frac{da}{dN}\right)^t = B(\Delta J^f)^m + \int [A(\Delta J^c)^n] dt \quad (8)$$

where the material constants *B, m* are for fatigue and *A, n* are for creep, ΔJ is the updated *J*-Integral range. The relation can be re-described for a symmetric, triangular waveform with an optional hold time (dwell period) at maximum load as [29]:

$$\left(\frac{da}{dN}\right)^t = B(\Delta J^f)^m + A(\Delta J^c)^n \left[\frac{Z}{w(n+1)} + \frac{t_{hold}}{(1-R)^n}\right] \quad (9)$$

where *R* is the load ratio (*R-ratio*) and Z is defined as:

$$Z = \frac{1 - R^{n+1}}{(1-R)^{n+1}} \quad (10)$$

In Eq. (9), the first part of the crack growth rate per cycle formulation (*da/dN*) governs the fatigue contribution and the latter part accounts for creep. The crack growth rate description includes the magnitude of the cyclic J-Integral parameter (ΔJ) that is analogous to the SIF, the frequency of the waveform, hold time at maximum load, the load ratio, and the temperature level.

2.4.4 XFEM implementation

Fracture mechanics related problems remain a challenge in the numerical simulations by its complicated nature to serve as a reliable tool in the industrial perspective. In the classical numerical approach, since the nodal shape functions for the finite element approximations represent discontinuities in the pre-constructed mesh, the fracture model restricts the crack growth along the predefined element boundaries. Mesh updating and treating the crack tip with special purpose elements can overcome the discontinuities and singularities reflected by the modelling part and its features. However, re-projecting the solution on the re-meshed field of interest in each crack propagation step and constructing a solution mosaic from the sub-steps can significantly increase the computation cost and influence the accuracy of the results.

A relatively recent approach XFEM, which is a numerical technique based on partition of unity method, enables modelling crack domains in engineering component analysis without explicitly meshing the crack surface [31-37]. The XFEM method creates a new displacement-field approximation by enriching the FEM approximation. The key idea is to extend the

conventional formulation by enrichment functions and model a discontinuity inside an element by adding shape functions to the finite element approximation. The initial crack geometry is typically represented implicitly by so-called level set method that tracks moving interfaces [38-40]. The mesh is independently generated from the crack geometry and the elements of the meshed structure does not necessarily need to conform to the crack surfaces. The convergence rate is improved for the solution by crack-tip enrichment. The displacement approximation for modelling the crack takes the new form, $\boldsymbol{u}_{xfem}$ by enriching the classical FE approximation, $\boldsymbol{u}_{fem}$.

$$\mathbf{u}_{fem}(x) = \sum_{i \epsilon L} N_i(x) u_i \tag{11}$$

$$\mathbf{u}_{\boldsymbol{xfem}}(\boldsymbol{x}) = \sum_{\boldsymbol{i \epsilon L}} \boldsymbol{N_i(x) u_i} + \sum_{\boldsymbol{i \epsilon M}} \boldsymbol{N_i(x) H(x) a_i} + \sum_{\boldsymbol{i \epsilon N}} \left[\boldsymbol{N_i(x)} \sum_{\boldsymbol{\alpha=1}}^{\boldsymbol{4}} \boldsymbol{F_\alpha(x)\, b_{i\alpha}} \right] \tag{12}$$

where *L*, *M*, and *N* are the set of all nodes, respectively, for the classical finite element, whose support is bisected by the crack, containing all the nodes of the crack tip elements; $N_i(x)$ is the shape function associated with node *i*, *H(x)*, the Heaviside function and F_a, the crack tip functions are the enrichments functions. The function introduces the discontinuity across the crack faces; *H(x)* is defined as; $H(x) = 1$ for $x > 0$ and -1 for $x < 0$. The crack tip is represented by four enrichment functions $(F_{a=1\text{-}4})$ to span the asymptotic near-tip displacement field of the Westergaard solution for an isotropic elastic material [32]:

$$[F_\alpha(r,\theta), \alpha = 1-4] = \left[\sqrt{r}\sin\frac{\theta}{2}, \sqrt{r}\cos\frac{\theta}{2}, \sqrt{r}\sin\theta\sin\frac{\theta}{2}, \sqrt{r\sin\theta}\cos\frac{\theta}{2}\right] \tag{13}$$

where (r,θ) belongs to the polar coordinate system having the origin at the crack tip and tangent to the crack at its tip at $\theta=0$.

3 Results

In this section, the experimental and the numerical results are presented. Firstly, the test combustor operating points are characterized and depicted as the stability map. The measured surface temperature and pressure profile in the downstream region are shown. Next, the prediction of the stress concentration location on the flame-box specimen by the thermal-structural coupled analysis is presented. Subsequently the results of the XFEM-based fracture mechanics analysis for the introduced crack are shown. Consequently the fatigue and creep contributions to the remaining lifing are described.

3.1 Combustion characterisation

The stability map was constructed for the test combustor and presented in Figure 4. The diamond markers represent the stable and the square markers are for the unstable combustion with respect to the initial settings such as the air/fuel ratio and the thermal power. There is a clear transition to generate the combustion instability mainly depending on the air/fuel ratio that the air fed into the system is reduced at a ratio to the fuel of 1.4. The power of 60 kW and the air/fuel ratio of 1.2 were selected as the extreme case within the test points for further investigation in this work that can be seen at the down-right corner in the stability map. This operating point will be denoted as Case6012 in the rest of the paper.

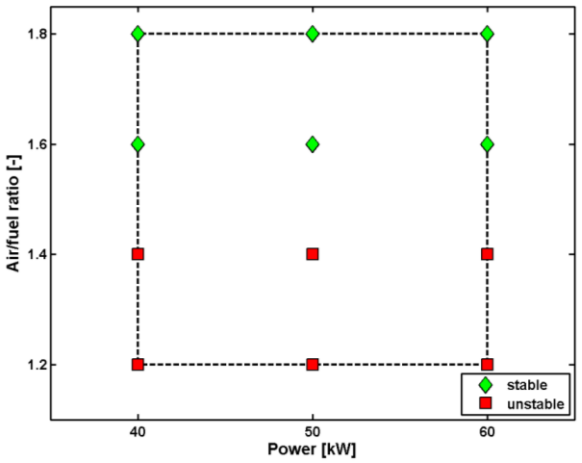

Figure 4. Combustor stability map

In Figure 5, the pressure spectrum is shown for the sample operating points including two unstable and two stable cases. The unstable cases shows a distinct pressure peak at a characteristic combustion frequency. The sub-harmonics of the characteristic frequency, at where the first peak stands, were generated due to the non-linear effects of the instability.

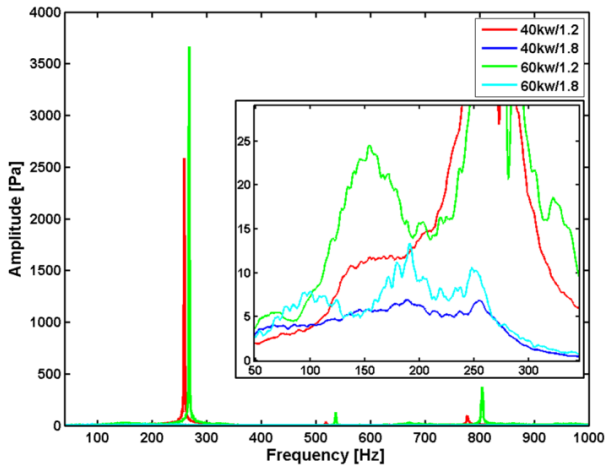

Figure 5. Pressure spectrum at p2 location.

The pressure amplitudes for the unstable cases are more than 100 times of the amplitudes for the stable cases. In Case6012, the pressure in the combustor ranges from 2130Pa to 3663Pa and the surface temperature of the liner ranges from 601.5°C to 301.5°C. Previous experiments showed that the temperature and pressure loads at the flame-box region were found to be sufficiently close to the measurements at the '*p2*' location. The loads along the downstream are depicted in Figure 6. These data were post-processed to be compatible for importing in the created mesh in the thermal-structural coupled analysis.

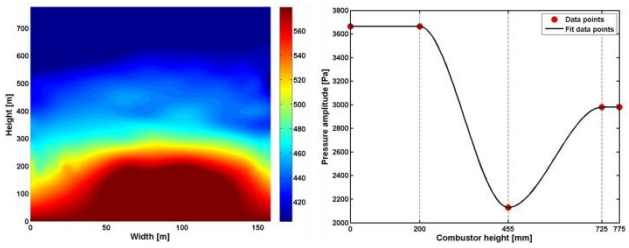

Figure 6. Downstream surface temperature and pressure profile

3.2 Temperature-structural analysis

The temperature and pressure profile in the downstream part of the combustor at Case6012 is presented in Figure 7 (a) and (b). In the figure, the highest temperature and pressure amplitudes are present at the flame-box region and the specimen is exposed to nearly-constant load amplitudes. Initially, a numerical test was carried out to compare the full-model and the sub-model results. In the analysis, the stress and strain distribution on the specimen geometry was found to be identical for the two numerical tests that implies the high stiffness of the flame-box structure. Thus, the further investigation was performed in the sub-model in order to reduce the computational cost.

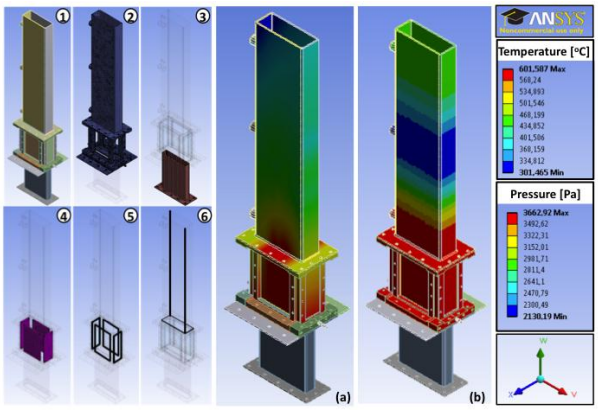

Figure 7. FEM modelling

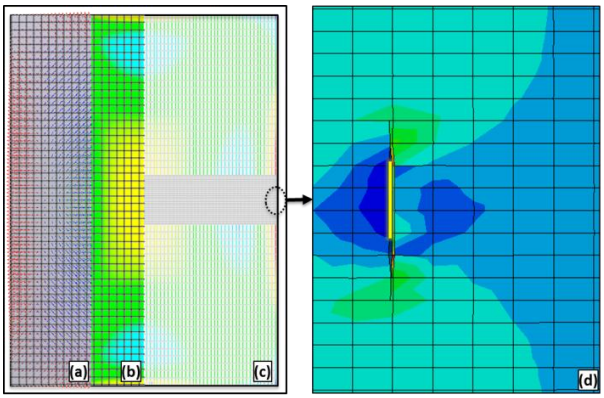

Figure 8. The stress distribution and crack growth

The stress distribution of the sub-model was calculated by the temperature-structural analysis presented in Figure 8 (left-background). This shows that the out-of-plane stresses are concentrated near the long edge sections. In the Figure 8, the maximum principal stress directions were calculated in the FEM mesh (b) and they are indicated with red arrows (a). The calculated stress field was transferred to the fracture mechanics analysis and a new mesh was generated for the XFEM analysis (d). In the

XFEM analysis, an initial slot-type crack (yellow-line) was located in the maximum stress region assuming that the crack propagation direction will be perpendicular to the calculated principal stress directions. Hence, the slot crack is placed at the mid-height near the longitudinal edge (0.5 mm from the edge) and it is aligned along this edge with 1 mm artificial initial crack length.

3.3 Residual lifing

In this section, the crack tip parameters relevant to crack growth are presented. In Figure 9, the J-Integral, which characterises the energy release rate associated with the crack growth, was calculated with respect to the near-tip field calculation contours at three levels (nodes) across the specimen thickness. These levels are designated as the *level-in*, *level-mid* and *level-out*. The level-in and level-out are the outer surface layers of the geometry that experience compression and tension stresses due to the cyclic motion of the specimen. Therefore, although the amplitudes, belong to the level-out, are higher than the amplitudes of the level-in, they swap each other during one cycle depending on the condition that the surface is under tension or compression stresses. An optimum number of contours were found to be six to capture the stress field spread around the crack tip. Thus, the crack-tip characterizing parameters are averaged with respect to the level-layers and the contours for the following calculations.

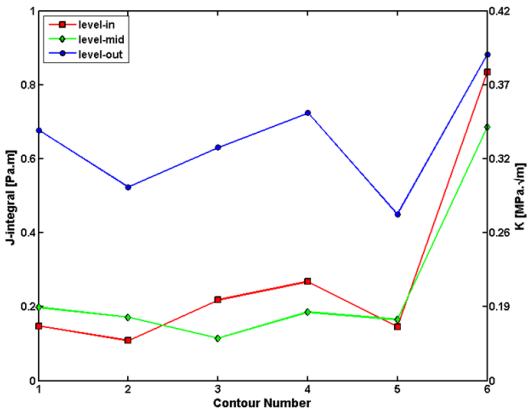

Figure 9. J-Integral convergence in calculation contours for the thickness

The experimentally measured pressure amplitude (3663Pa) was found to be insufficient to cause crack propagation. Therefore, three higher pressure amplitudes, were included in the investigation for the comparison. These four pressures will be called as the numerical test pressures that are 3663Pa, 36630Pa, 366300Pa, 3663000Pa.

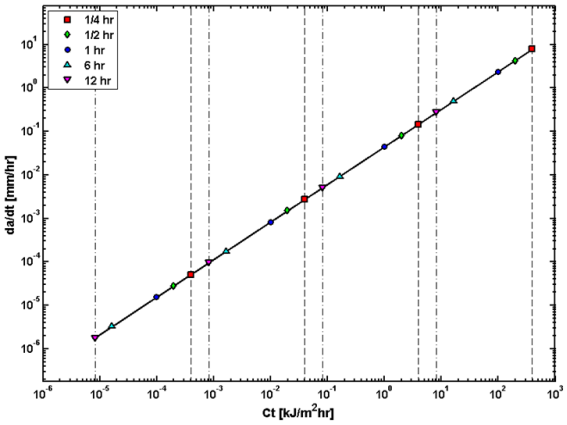

Figure 10. Unit time crack growth rates as a function of C_t

Assuming that the crack growth is governed by a modified Paris-Erdogan law-type model (Eq. (7)), the crack growth rate is proportional to the SIF and J-integral, and hence the C_t-Integral. Thus, the remaining life is covered by the inverse-relation to the C_t-Integral. In Figure 10, the plot is divided into 4 regions. Each region starts with dash-dot line and ending with dashed line. The marker-data, delimited by the lines within these regions, belong to the numerical test pressures (ascending from left to right). The lifetime and C_t relation shows that the increase in the pressure, thus the increase in C_t, increases the crack growth rate and decreases the lifetime. The hold-time promotes the intergranular fracture mode changing from transgranual as in pure fatigue fracture mode [12]. This indicates that the time-dependent damage mechanisms related to the creep crack growth are in control as the holding time introduced instead of the cycle-dependent mechanisms.

4 Concluding remarks and discussions

The following conclusions are mainly drawn over this work:

- A laboratory-scaled generic gas turbine combustor was designed to investigate the

structural dynamics due to the combustion instabilities.

- Particularly, nickel-based super alloy material was of interest that is relevant to typical gas turbine hot section components. Thus, the experimental output was projected on the numerical analysis. Haynes 230 was chosen as the material to investigate the structural characteristics at elevated temperature.

- The possible cracking region was predicted by temperature-structural analysis. Subsequently, the XFEM technique was applied for the crack modelling and analysis under the assumption of small scale yielding conditions. The advancement of the crack quantified by the C_t-integral evaluation which represents the fatigue and creep contributions.

- Since the pressure generated due to combustion process is in cyclic manner, the stresses will vary between tensile and compressive types. This will promote the crack to grow at both sides and eventually through thickness. The acoustic volume in the flame-box expands and contracts due to the pressure oscillations that result the cyclic loadings of the plate and its relative motion. This will enable the crack to open at outer face at the volume expansion and to close at the volume contraction. Thus, the total remaining lifetime of the through thickness crack would be the half of the calculated lifetime due to this cyclic or sequential crack growth at the two sides of the plate.

- Note that the experimentally measured mechanical and thermal loads driven by the unstable combustion process was used in the numerical analysis to characterize the crack parameters. Hence, the numerical fracture mechanics analysis must be validated by experiments. Therefore, an unconventional test system design is required to cover the fatigue/creep aspects of the combustor structure instead of the standard specimens.

Acknowledgments

The research is funded by the EC in the Marie Curie Actions – Networks for Initial Training, under call FP7-PEOPLE-2007-1-1-ITN, Project LIMOUSINE with project number 214905.

References

[1] Cruse, T. A., Mahadevan, S., and Tryon, R. G., 1997, "Fatigue Reliability of Gas Turbine Engine Structures," Technical Report No. NASA,

[2] Tryon, R. G., Cruse, T. A., and Mahadevan, S., 1996, "Development of a Reliability-Based Fatigue Life Model for Gas Turbine Engine Structures," Engineering Fracture Mechanics, 53(5), pp. 807-828.

[3] Yang, J. N., 1994, "Application of Reliability Methods to Fatigue, Quality Assurance and Maintenance," Structural Safety & Reliability, Vols 1-3, pp. 3-18.

[4] Haynes International, 2007, "Haynes 230 Alloy Product Brochure, H-3000: www.haynesintl.com," Technical Report No.

[5] Ansys® Academic Research, Release 14.0, ANSYS, Inc., Theory Reference.

[6] Davis, J. R., 1997, *Heat-Resistant Materials*, *Asm Specialty Handbook*, ASM International, Materials Park, Ohio.

[7] Hutchinson, J. W., 1968, "Singular Behaviour at the End of a Tensile Crack in a Hardening Material," Journal of the Mechanics and Physics of Solids, 16(1), pp. 13-31.

[8] Rice, J. R., and Rosengren, G. F., 1968, "Plane Strain Deformation near a Crack Tip in a Power-Law Hardening Material," Journal of the Mechanics and Physics of Solids, 16(1), pp. 1-12.

[9] Curbishley, I., Pilkington, R., and Lloyd, G. J., 1986, "Macroscopic Creep Crack Growth in Type 316 Stainless Steel.: Iii. Application of Linear and Nonlinear Elastic Fracture Mechanics," Engineering Fracture Mechanics, 23(2), pp. 401-422.

[10] Saxena, A., 1980, "For the Characterization of Creep-Crack-Growth Behavior in 304 Stainless Steel," eds., St Louis, MO, USA, pp. 131-151.

[11] Fu, L. S., 1980, "Creep Crack Growth in Technical Alloys at Elevated Temperature—a Review," Engineering Fracture Mechanics, 13(2), pp. 307-330.

[12] Lu, Y. L., Liaw, P. K., Sun, Y., Wang, G. Y., Thompson, S. A., Blust, J. W., Browning, P. F., Bhattacharya, A. K., Aurrecoechea, J. M., and Klarstrom, D. L., 2007, "Hold-Time Effect on the Elevated-Temperature Crack Growth Behavior of Solid-Solution-Strengthened Superalloys," Acta Materialia, 55(3), pp. 767-775.

[13] Lu, Y. L., Liaw, P. K., Chen, L. J., Wang, G. Y., Benson, M. L., Thompson, S. A., Blust, J. W., Browning, P. F., Bhattacharya, A. K., Aurrecoechea, J. M., and Klarstrom, D. L., 2006, "Tensile-Hold Effects on High-Temperature Fatigue-Crack Growth in Nickel-Based Hastelloy® X Alloy," Materials Science and Engineering: A, 433(1–2), pp. 114-120.

[14] Riedel, H., 1981, "Creep Deformation at Crack Tips in Elastic-Viscoplastic Solids," Journal of the Mechanics and Physics of Solids, 29(1), pp. 35-49.

[15] Saxena, A., 1984, "Creep Crack-Growth under Non Steady-State Conditions," Journal of Testing and Evaluation, 12(4), pp. 191-192.

[16] Saxena, A., 1991, "Creep Crack-Growth in High-Temperature Ductile Materials," Engineering Fracture Mechanics, 40(4-5), pp. 721-736.

[17] Grover, P. S., and Saxena, A., 1995, "Creep Crack-Growth in Power-Plant Materials," Sadhana-Academy Proceedings in Engineering Sciences, 20(pp. 53-85.

[18] Saxena, A., 1997, "Creep-Fatigue Crack Growth in Power-Plant Materials and Components," Advances in Fracture Research, Vols 1-6, pp. 51-62.

[19] Saxena, A., Ernst, H. A., and Landes, J. D., 1983, "Creep Crack Growth Behavior in 316 Stainless Steel at 594°C (1100°F)," International Journal of Fracture, 23(4), pp. 245-257.

[20] Riedel, H., and Rice, J. R., 1980,

[21] Hamilton, B. C., Hall, D.E., Saxena, A., Mcdowell, D.L. , 1997, "Creep Crack Growth Behavior of Aluminum Alloy 2519: Part I - Experimental Analysis," eds., Philadelphia, PA, pp. 3-18.

[22] Hall, D. E., Hamilton B.C., Mcdowell, D.L., Saxena A., 1997, "Creep Crack Growth Behavior of Aluminum Alloy 2519: Part I - Numerical Analysis," eds., Philadelphia, PA, pp. 19-36.

[23] Sadananda, K., and Shahinian, P., 1981, "Review of the Fracture-Mechanics Approach to Creep Crack-Growth in Structural Alloys," Engineering Fracture Mechanics, 15(3-4), pp. 327-342.

[24] Saxena, A., 1991, "Creep Crack Growth in High Temperature Ductile Materials," Engineering Fracture Mechanics, 40(4–5), pp. 721-736.

[25] Kuo, A.-Y., Chen, K.-L., Saxena, A., and Nagar, A., 1992, "An Integral Formulation of Ct for Use in Creep Crack Growth Evaluation," International Journal of Fracture, 57(3), pp. 269-280.

[26] Bassani, J. L., and Mcclintock, F. A., 1981, "Creep Relaxation of Stress around a Crack Tip," International Journal of Solids and Structures, 17(5), pp. 479-492.

[27] Bassani, J. L., Hawk, D. E., and Saxena, A., 1989, Nonlinear Fracture Mechanics: Time-Dependent Fracture, Volume I, (Astm Stp 995), American Society for Testing and Materials, Philadelphia, PA, Evaluation of the Ct Parameter for Characterizing Creep Crack Growth Rate in the Transient Regime.

[28] Saxena, A., 1980, "A Model for Predicting the Effect of Frequency on Fatigue Crack Growth Behavior at Elevated Temperature," Fatigue & Fracture of Engineering Materials & Structures, 3(3), pp. 247-255.

[29] Gayda, J., Gabb, T. P., and Miner, R. V., 1988, Fatigue Crack Propagation of Nickel-Base Superalloys at 650°C, American Society for Testing and Materials, Philadelphia, Low Cycle Fatigue (Astm Stp 942).

[30] Zhang, G., Yuan, H., and Li, F., 2012, "Analysis of Creep–Fatigue Life Prediction Models for Nickel-Based Super Alloys," Computational Materials Science, 57(0), pp. 80-88.

[31] Babuška, I., and Melenk, J. M., 1997, "The Partition of Unity Method," International Journal for Numerical Methods in Engineering, 40(4), pp. 727-758.

[32] Belytschko, T., and Black, T., 1999, "Elastic Crack Growth in Finite Elements with Minimal Remeshing," International Journal for Numerical Methods in Engineering, 45(5), pp. 601-620.

[33] Bordas, S., Nguyen, P. V., Dunant, C., Guidoum, A., and Nguyen-Dang, H., 2007, "An Extended Finite Element Library," International Journal for Numerical Methods in Engineering, 71(6), pp. 703-732.

[34] Daux, C., Moës, N., Dolbow, J., Sukumar, N., and Belytschko, T., 2000, "Arbitrary Branched and Intersecting Cracks with the Extended Finite Element Method," International Journal for Numerical Methods in Engineering, 48(12), pp. 1741-1760.

[35] Fries, T.-P., and Belytschko, T., 2010, "The Extended/Generalized Finite Element Method: An Overview of the Method and Its Applications," International Journal for Numerical Methods in Engineering, 84(3), pp. 253-304.

[36] Melenk, J. M., and Babuška, I., 1996, "The Partition of Unity Finite Element Method: Basic Theory and Applications," Computer Methods in Applied Mechanics and Engineering, 139(1–4), pp. 289-314.

[37] Moës, N., Dolbow, J., and Belytschko, T., 1999, "A Finite Element Method for Crack Growth without Remeshing," International Journal for Numerical Methods in Engineering, 46(1), pp. 131-150.

[38] Gravouil, A., Moës, N., and Belytschko, T., 2002, "Non-Planar 3d Crack Growth by the Extended Finite Element and Level Sets—Part Ii: Level Set Update," International Journal for Numerical Methods in Engineering, 53(11), pp. 2569-2586.

[39] Stolarska, M., Chopp, D. L., Moës, N., and Belytschko, T., 2001, "Modelling Crack Growth by Level Sets in the Extended Finite Element Method," International Journal for Numerical Methods in Engineering, 51(8), pp. 943-960.

[40] Sukumar, N., Chopp, D. L., and Moran, B., 2003, "Extended Finite Element Method and Fast Marching Method for Three-Dimensional Fatigue Crack Propagation," Engineering Fracture Mechanics, 70(1), pp. 29-48.

Copyright Statement